Available online at www.sciencedirect.com
ScienceDirect
Journal of Inorganic Biochemistry 101 (2007) 1719–1729
Journal of Inorganic Biochemistry
www.elsevier.com/locate/jinorgbio

Structure and activity of apoferritin-stabilized gold nanoparticles

Lei Zhang, Joe Swift, Christopher A. Butts, Vijay Yerubandi, Ivan J. Dmochowski *

Department of Chemistry, University of Pennsylvania, 231 South 34th Street, Philadelphia, PA 19104-6323, USA

Received 28 March 2007; received in revised form 12 July 2007; accepted 13 July 2007
Available online 26 July 2007

We remember Ed Stiefel and thank him for turning us on to ferritin

Abstract

A simple method for synthesizing gold nanoparticles stabilized by horse spleen apoferritin (HSAF) is reported using $NaBH_4$ or 3-(*N*-morpholino)propanesulfonic acid (MOPS) as the reducing agent. $AuCl_4^-$ reduction by $NaBH_4$ was complete within a few seconds, whereas reduction by MOPS was much slower; in all cases, protein was required during reduction to keep the gold particles in aqueous solution. Transmission electron microscopy (TEM) showed that the gold nanoparticles were associated with the outer surface of the protein. The average particle diameters were 3.6 and 15.4 nm for $NaBH_4$-reduced and MOPS-reduced Au-HSAF, respectively. A 5-nm difference in the UV–Vis absorption maximum was observed for $NaBH_4$-reduced (530 nm) and MOPS-reduced Au-HSAF (535 nm), which was attributed to the greater size and aggregation of the MOPS-reduced gold sample. $NaBH_4$-reduced Au-HSAF was much more effective than MOPS-reduced Au-HSAF in catalyzing the reduction of 4-nitrophenol by $NaBH_4$, based on the greater accessibility of the $NaBH_4$-reduced gold particle to the substrate. Rapid reduction of $AuCl_4^-$ by $NaBH_4$ was determined to result in less surface passivation by the protein. Methods for studying ferritin–gold nanoparticle assemblies may be readily applied to other protein–metal colloid systems.
© 2007 Elsevier Inc. All rights reserved.

Keywords: Horse spleen apoferritin; Gold; Nanoparticle; $NaBH_4$; 3-(*N*-morpholino)propanesulfonic acid; Protein template; Catalysis

1. Introduction

Biomolecule-inorganic nanoparticle assemblies are the subject of growing research, and have become important for advances in catalysis, sensing, optoelectronics and biomedical applications. Biomolecules such as oligonucleotides [1–8], peptides [9–12], and proteins [13–17] offer rich structural and functional diversity for synthesizing inorganic nanoparticles of different compositions, sizes, and shapes, and controlling their arrangement into complex architectures [18,19]. The need for more sensitive bioanalytical assays have made gold nanoparticles a particular focus of current research [20–29]. Gold nanoparticles are useful for applications such as colorimetric sensing [30–32], contrast-enhanced optical imaging [33], and photothermal therapy [34], based on strong absorption from the gold surface plasmon resonance (SPR) band, which is sensitive to local environment [35–37]. For uses of gold nanoparticles in aqueous solutions, it is important to enhance physicochemical stability and solubility through passivation of the gold surface.

We chose horse spleen apoferritin (HSAF) as the passivating agent, because unlike commonly used stabilizers, apoferritin is comprised of 24 four-helix bundles that self assemble to form a 12-nm spherical protein with an 8-nm diameter cavity. We show in this work that gold nanoparticles form on the outer protein surface, leaving the cavity empty for subsequent reactions. The differential reactivity of HSAF interior and exterior surfaces, and the ability to store small molecules within the protein cavity [38–40], provide opportunities to fabricate multifunctional nanomaterials with controlled molecular features. It is well known that HSAF can react with Fe^{2+} and dioxygen to store as many as 4000 Fe^{3+} ions as a ferrihydrite core within its interior [41]. Apoferritin also templates the synthesis of

* Corresponding author. Tel.: +1 215 898 6459; fax: +1 215 898 2037.
E-mail address: ivandmo@sas.upenn.edu (I.J. Dmochowski).

0162-0134/$ - see front matter © 2007 Elsevier Inc. All rights reserved.
doi:10.1016/j.jinorgbio.2007.07.023

various inorganic particles, including metals, metal oxides, and semiconductors [42]. Growth of particles inside apoferritin requires addition of metal ions together with a reductant. The protein shell is perforated by narrow hydrophilic channels at the 3-fold symmetry axes that are believed to promote the transport of metal ions into the cavity [15,43,44]. Previous studies have added metal ranging from a few hundred to several thousand ions per HSAF holoprotein, as summarized in Table 1. Transmission electron microscopy (TEM) data indicated that the nanoparticles typically grew inside the apoferritin cavity. Importantly, the metal ion sources were divalent cations, with two exceptions being Cr^{3+} and Au^{+} [45,46]. Although the formation of Au_2S nanoparticles inside HSAF was recently described [45,46], the present study is the first detailed report on the addition and reduction of Au^{3+} to form Au^0 nanoparticles outside of HSAF. The main goal in the present manuscript is not to prepare efficient biocatalysts but to get a fundamental understanding about the gold-HSAF system, how HSAF stabilizes gold particles, and how one of the synthetic routes used gives better surface passivation, while the other gives better access to reactants so that gold can still participate in catalysis. We elucidated the structure and activity of ferritin–gold nanoparticles formed under various reaction conditions. Methods for characterizing these protein–gold assemblies may be applied to other bio-inorganic systems.

Several groups have sought to develop methods for preparing spherical gold particles in a range of diameters [37,47–50], as important physical properties vary with the dimensions of the gold [35]. The SPR maximum is normally between 520 and 530 nm for spherical gold particles less than 20 nm in diameter, but this absorption feature can vary widely, depending on the size, aspect ratio, and aggregation state, and chemical environment of the particles [19]. Whetten and colleagues studied the absorption spectra of a series of nanocrystalline gold particles, and found that the SPR band became identifiable only for structures greater than 2.0 nm in diameter [35]. Researchers have employed capping agents, such as alkanethiols, surfactants, peptides, or proteins, in order to confine gold particle growth on the nanoscale and passivate the surface [19]. One example is the globular protein bovine serum albumin (BSA) [51–53]. The José-Yacamán group reported the synthesis of gold nanoparticles smaller than 2 nm through $NaBH_4$ reduction in the presence of BSA. This eliminated the need for stabilizing agents, such as citrate, or linker molecules, such as glutaric dialdehyde [51]. Using a different approach, Singh et al. produced gold nanoparticles by *in situ* reduction of gold ions in a foam generated by passing N_2 gas through a BSA solution [52]. The protein played a role as both foaming and stabilizing agent. The photoreduction of gold nanoparticles in the presence of BSA has also been described, and it was noted that in addition to BSA, several other proteins can stabilize the gold [53]. Besides the use of proteins, water-soluble, biocompatible gold nanoparticles of different sizes have also been synthesized using dendrimers [54], and short peptides such as tiopronin [37] and glutathione as capping agents [55], as well as a dodecapeptide identified from a phage display library [56].

In a broad context, apoferritin serves as a useful paradigm for studying protein–metal nanoparticle interactions. We found that upon reduction of several thousand equivalents of $AuCl_4^-$ in the presence of HSAF, apoferritin-stabilized the gold particles in aqueous solution through exterior surface interactions. This is similar to copper-HSAF systems, where Cu^0 particles larger than the ferritin cavity were stabilized by the protein in water [57]. We report several methods for probing protein–gold assemblies and compare the properties of Au-HSAF particles synthesized under different conditions. Key features of the gold–apoferritin complexes, such as stability and particle morphology, were affected by the nucleation, growth, and final passivation of the particles, which varied with the reaction conditions. We begin to consider these factors in this work.

Table 1
Literature survey of inorganic complexes formed with horse spleen apoferritin (HSAF)

Material	Metal ion source	Metal:HSAF ratio[a]	Reference
Metals			
Pd	$PdCl_4^{2-}$	500	[68]
Cu	Cu^{2+}	225	[69]
Co	Co^{2+}	Not specified	[70]
Ni	Ni^{2+}	Not specified	[70]
Metal oxides, hydroxides, and oxyhydroxides			
FeOOH	Fe^{2+}	4500	[71]
Fe_3O_4	Fe^{2+}	3000	[72]
U oxide	UO_2^{2+}	4000	[73]
U oxo complex	UO_2^{2+}	800	[74]
MnOOH	Mn^{2+}	3000	[75]
MnOOH	Mn^{2+}	1200	[76]
CoOOH	Co^{2+}	2250	[77]
CoOOH	Co^{2+}	1500	[76]
Cr hydroxide	Cr^{3+}	4800	[45]
Ni hydroxide	Ni^{2+}	8000	[45]
Semiconductors			
CdS	Cd^{2+}	55–275	[78]
CdSe	Cd^{2+}	1000	[79]
ZnSe	Zn^{2+}	1500	[80]
Au_2S	Au^{+}	3000	[46]

[a] Number indicates initially added metal ions per HSAF 24-mer protein.

2. Experimental design

2.1. Reagents

All chemicals were of analytical reagent grade and used without further purification, unless otherwise stated. *Sigma*: horse spleen apoferritin (obtained as a 53 mg/mL, 0.1 M NaCl solution); horse spleen ferritin (HSF, obtained as an 85 mg/mL, 0.15 M NaCl solution); 3-(*N*-morpholino)propanesulfonic acid (MOPS). *Fisher*: hydrogen tetrachloroaurate(III) hydrate ($HAuCl_4 \cdot xH_2O$, p.a.). *Acros:* gold(III) chloride ($AuCl_3$), and 4-nitrophenol. *Aldrich:*

sodium borohydride ($NaBH_4$). All solutions were prepared using deionized water purified by ultrapure water systems.

2.2. Sample preparation

$AuCl_4^-$ was used as the gold ion source, while $NaBH_4$ or MOPS was used as the reducing agent. $AuCl_3$ was also tested as the gold ion source following the same synthetic procedure. HSAF (3.79 μL, 0.11 mM) was dissolved in a 2-mL buffer solution (0.4 M NaCl, 0.1 M KH_2PO_4, pH 7.5). 16.66 μL of 0.1 M $AuCl_4^-$ (4000 eq per HSAF) was added and the mixture was stirred for 1 h at rt. 50 μL of 0.1 M $NaBH_4$ (3 eq per $AuCl_4^-$) or 83.3 μL of 1 M MOPS (50 eq per $AuCl_4^-$) was then added to reduce the gold ions and the resulting solution was stirred for 1 h. This solution was centrifuged at 5000 rpm for 10 min (Eppendorf Centrifuge 5415D). The Au-HSAF product was subsequently passed through a gel filtration column (Econo-Pac 10DG column, Bio-Rad; eluent: 0.4 M NaCl, 0.1 M KH_2PO_4, pH 7.5).

2.3. Physical measurements

UV–visible (UV–Vis) absorption spectra and kinetics monitoring absorption changes were recorded on an Agilent 8453 UV–Vis spectrophotometer with temperature controller (25 °C) and magnetic stirrer (300 rpm, Agilent 89090A), using a quartz cuvette with 1-cm path length. Chemical reactions were monitored at 530 nm to track the SPR band associated with gold particle formation. Circular dichroism (CD) measurements were obtained on a polarimeter (AVIV, model 62A DS) in the temperature range of 4–96 °C with a 1-mm path length optical cell. High-resolution TEM data and images were collected using a JEOL 2010F TEM with 0.23 nm point-to-point resolution at the Penn Regional Nanotechnology Facility. Low-resolution TEM data and images were collected at the Penn Biomedical Imaging Facility. Inductively coupled plasma optical emission spectroscopy (ICP-OES) was performed by Galbraith Laboratories, Inc. to determine the gold stoichiometry of Au–ferritin samples in solution. The Bio-Rad Protein Assay, based on the Bradford method [58], was used to determine the concentration of HSAF.

2.4. Fast protein liquid chromatography (FPLC)

HSAF solution (2 mL, 0.208 μM) was stirred with $AuCl_4^-$ (41.6 μL, 0.1 M) before adding $NaBH_4$ (124.8 μL, 0.1 M). Following reduction for 1 h, the sample was divided into four equal portions and additional HSAF solution was added to three of those portions, to achieve a final HSAF concentration of 0.417 μM, 0.833 μM and 1.875 μM. The samples were then left at 4 °C overnight, centrifuged at 5000 rpm for 10 min, and passed through a Superdex S200 column (Akta FPLC system, GE Healthcare) running 0.15 M NaCl, 0.02 M Tris, pH 7.4 buffer (TBS) and monitoring absorption at 280 nm.

In a parallel experiment, HSAF solution (2 mL, 0.208 μM) was stirred with $AuCl_4^-$ (41.6 μL, 0.1 M) before adding MOPS (208 μL, 1 M). Following reduction for 1 h, the sample was divided into three equal portions and more HSAF was added to two of these portions, to achieve a final HSAF concentration of 0.417 μM and 0.833 μM. The samples were then left at 4 °C overnight, centrifuged at 5000 rpm for 10 min, and passed through a Superdex S200 column running TBS and monitoring absorption at 280 nm. The Superdex S200 column was calibrated by using high molecular weight standards as described in the manufacturer's protocol.

2.5. Catalytic properties

The reduction of 4-nitrophenol by $NaBH_4$ in the presence of Au-HSAF catalyst was studied in 2-mL solutions, with an identical procedure for $NaBH_4$-reduced and MOPS-reduced Au-HSAF. In a standard quartz cell with a 1-cm path length, 50 μL of 0.1 M $NaBH_4$ was mixed with 0.5 mL of 0.2 mM 4-nitrophenol. 1.25 mL of H_2O was then added. UV–Vis measurements were initiated with the addition of 0.2 mL of 50 nM Au-HSAF solution. For experiments measuring the effects of extra HSAF on catalytic activity, 3, 10, or 30 μL of 10 μM HSAF were premixed with Au-HSAF solution and then added together to the solution mixture of 4-nitrophenol and $NaBH_4$. The kinetics of 4-nitrophenol reduction were monitored by UV–Vis spectroscopy, with spectra recorded at 15-s intervals in a scanning range of 200–800 nm at 25 °C.

2.6. Effect of reaction time on catalysis

$NaBH_4$- or MOPS-reduced Au-HSAF samples were prepared following the synthetic procedure specified in Section 2.2, the only difference being that after adding $NaBH_4$ or MOPS, the resulting solution was stirred for up to 24 h. The concentrations of the Au-HSAF samples were adjusted to reach the same absorption intensity at 530 nm ($OD_{530nm} = 0.66$). To study the effect of reaction time on catalysis, in a standard quartz cell with a 1-cm path length, 50 μL of 0.1 M $NaBH_4$ was mixed with 0.5 mL of 0.2 mM 4-nitrophenol. 1.25 mL of H_2O was then added. UV–Vis measurements were initiated with the addition of 0.2 mL of the above Au-HSAF solution. The kinetics of 4-nitrophenol reduction were monitored by UV–Vis spectroscopy, with spectra recorded at 15-s intervals in a scanning range of 200–800 nm at 25 °C.

3. Results and discussion

During sample preparation, HSAF was first stirred for 1 h with 4000 eq $AuCl_4^-$ at 25 °C to afford a clear, pale yellow solution. No gold was observed to precipitate during this mixing process. The gold ions were then reduced by $NaBH_4$ (3 eq per $AuCl_4^-$) or MOPS (50 eq per $AuCl_4^-$) to yield Au^0 particles, and the solution became reddish-purple

during a 1-h reaction. Reduction times greater than 1 h led to decreased SPR band intensity. Au-HSAF was purified by gel filtration chromatography in ca. 30% ($NaBH_4$-reduced sample) and 50% (MOPS-reduced sample) overall yields, based on the starting quantity of HSAF, as determined by the Bio-Rad Protein Assay. ICP-OES measurements revealed that the average Au atom-to-HSAF 24-mer ratio was 1500:1.

High-resolution TEM was used to characterize the structure of the Au-HSAF samples. The TEM images (Fig. 1a and b) and the particle size histograms (Fig. 1c and d) showed broad particle size distributions with mean diameters of 3.6 ± 1.2 nm and 15.4 ± 4.5 nm for $NaBH_4$-reduced and MOPS-reduced Au-HSAF, respectively. Energy dispersive spectroscopy (EDS) positively identified gold in the nanoparticle samples (Fig. 1e). Particle atomic spacings were 0.245 nm (Fig. 1f). The lack of correlation between particle morphology (mean diameter and the range of sizes) and the 8-nm diameter apoferritin interior suggested that particle growth and stabilization did not occur within the protein cavity. The average diameter of MOPS-reduced gold particles was approximately twice the size of the 8-nm HSAF cavity, whereas the $NaBH_4$-reduced gold particles were less than half the diameter of the HSAF cavity. Fig. 2a shows a high-resolution TEM image of $NaBH_4$-reduced Au-HSAF, which was stained with 2% phosphotungstic acid (PTA). PTA was largely excluded from the HSAF interior, and therefore provided negative contrast for the protein. This TEM image provided strong evidence that even the smaller $NaBH_4$-

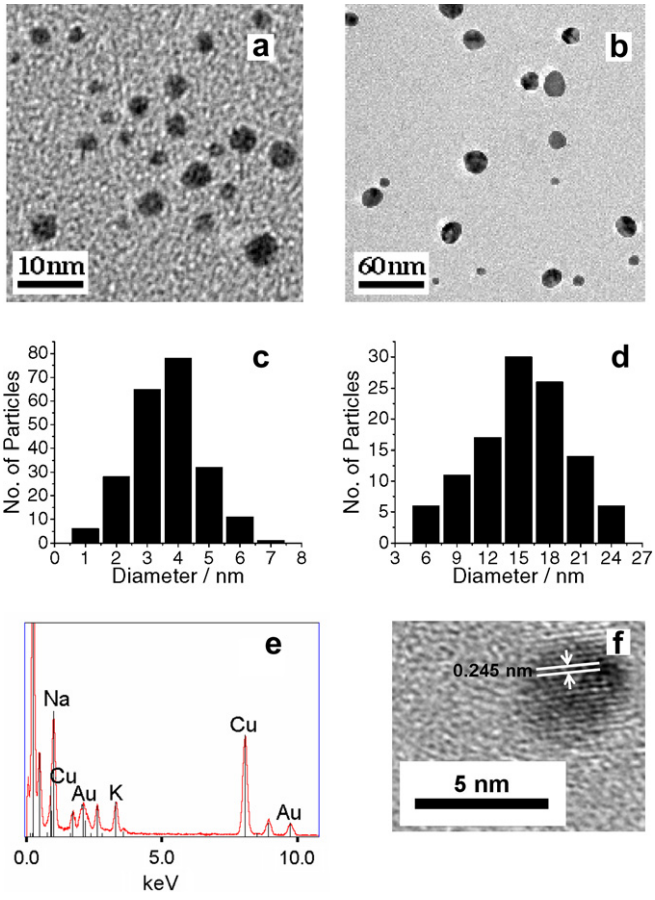

Fig. 1. (a) TEM image of Au-HSAF reduced by $NaBH_4$. (b) TEM image of Au-HSAF reduced by MOPS. (c) Histogram of the particle sizes of the sample in (a), 222 particles analyzed. (d) Histogram of the particle sizes of the sample in (b), 110 particles analyzed. (e) Energy dispersive spectrum of representative Au-HSAF sample placed on copper specimen grid. (f) The atomic gold lattice spacings of an Au-HSAF sample.

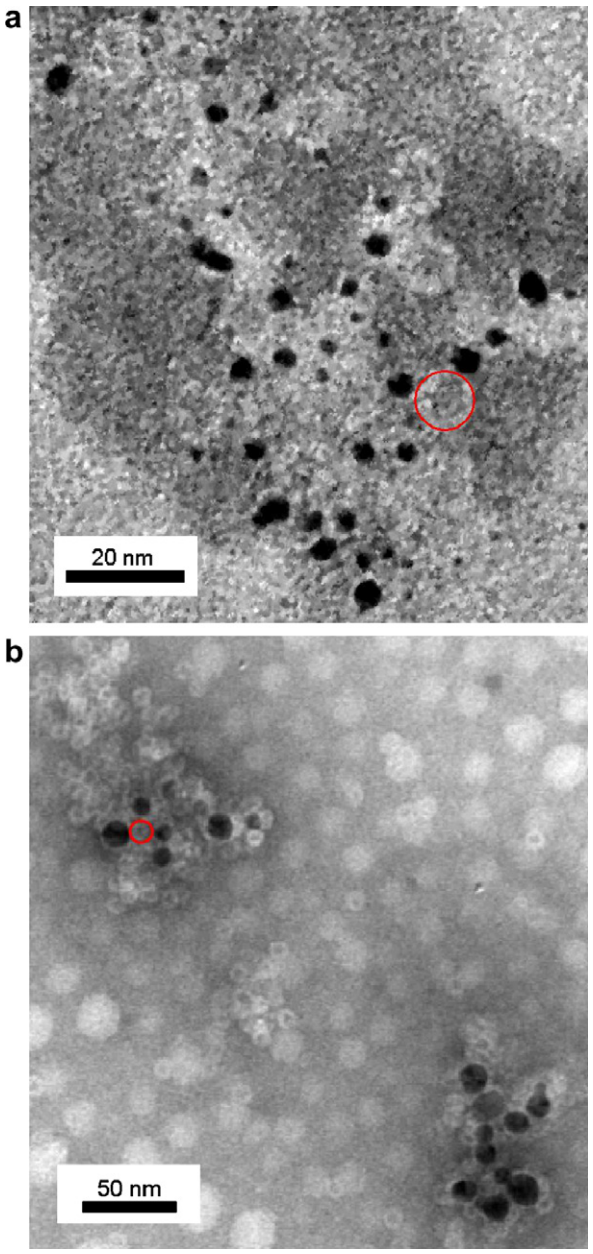

Fig. 2. TEM images showing gold nanoparticles (dark black circles) associated with the exterior surface of HSAF (white rings, examples outlined in red). $AuCl_4^-$ was reduced by (a) $NaBH_4$ or (b) MOPS, resulting in gold particles with different size distributions. 'a' was imaged at 200 kV using phosphotungstic acid (PTA) stain to create negative contrast for protein. 'b' was imaged at 120 kV using an uranyl acetate stain; the larger white circles are an artifact caused by the stain drying process.

reduced gold nanoparticles (black circles) did not form inside the cavity and were forced to reside at the outer HSAF surface (larger white circles). Similar results were obtained from low-resolution TEM images of MOPS-reduced Au-HSAF (Fig. 2b).

We postulate that the gold is binding with highest probability to amino acids with sulfur-, nitrogen-, and oxygen-containing side chains at pH 7.5, all of which are positioned prominently on the outer surface of HSAF. These residues are expected to bind gold ions, where gold is subsequently reduced and gold particles are nucleated on the outer protein shell. The anionic protein channels of ferritin promote the transport of divalent cations into the cavity (Table 1), but are not well suited to transport larger gold complexes that are neutral ($AuCl_3$) or mono-anionic ($AuCl_4^-$). Thus, in a competition between Au^{3+} binding and reduction at the outer ferritin surface and metal ion transport to the protein interior, it appears that most of the gold is reduced at residues on the protein exterior. Mutagenesis experiments are ongoing in our lab to probe gold–ferritin interactions more directly.

In addition to electrostatic considerations, we hypothesized that the different gold particle size distributions should relate to differences in the kinetics of gold particle formation. $NaBH_4$ is a strong reducing agent that rapidly reduced $AuCl_4^-$ and likely nucleated numerous particles, thereby depleting the gold salt before larger particles were able to form. MOPS is a much milder reducing agent, yielding slower gold particle nucleation and growth that were strongly mediated by the protein.

Fig. 3a shows the kinetics of $AuCl_4^-$ reduction by $NaBH_4$ in the presence and absence of HSAF, monitored at 530 nm. In both samples, the SPR band reached a maximum in 5 s, indicating kinetics at least as fast as the mixing time of our apparatus. In the absence of HSAF, the absorption was observed to decrease from its initial maximum due to the precipitation of gold colloid. However, the SPR band observed in the presence of HSAF remained unchanged, indicating that the gold nanoparticles were stabilized by the protein in solution. As a second control experiment, $AuCl_4^-$ was stirred with HSAF without the addition of the reducing agent $NaBH_4$ (Fig. 3a) or MOPS (Fig. 3b). $AuCl_4^-$ was not reduced on the same timescale of seconds-to-minutes, as evidenced by the lack of an SPR band.

In fact, with only HSAF as the reductant, the formation of gold nanoparticles required weeks of stirring in the dark. In parallel with these studies, we attempted to form gold nanoparticle–protein assemblies via a stepwise process of first reducing Au^{3+} (16.66 μL, 0.1 M) in solution with $NaBH_4$ (50 μL, 0.1 M) or MOPS (83.3 μL, 1 M) for 1 h and then adding HSAF (3.79 μL, 0.11 mM). The solution mixture was stirred for 1 h. Bulk gold precipitation was unambiguously observed, and the sequential addition of HSAF failed to produce soluble gold nanoparticles under these conditions.

Fig. 3b shows the kinetics of $AuCl_4^-$ reduction by MOPS in the presence and absence of HSAF, which occurred on

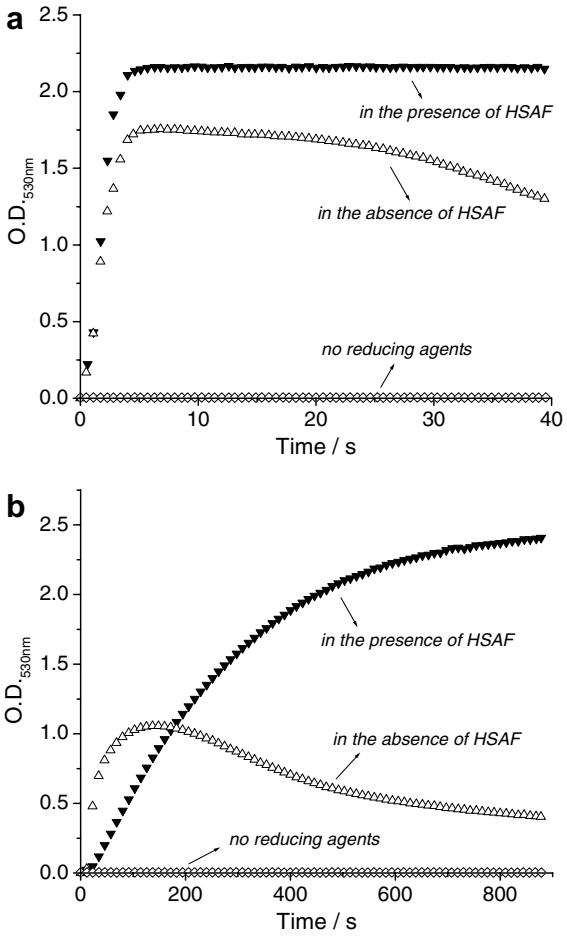

Fig. 3. (a) Kinetics traces of $AuCl_4^-$ reduction by $NaBH_4$ in the presence (▼) or absence (△) of HSAF. Kinetics trace of $AuCl_4^-$ stirred with HSAF without adding $NaBH_4$ (◇); no particle formation was observed to occur on this timescale. (b) Kinetics traces of $AuCl_4^-$ reduction by MOPS in the presence (▼) or absence (△) of HSAF. Kinetics trace of $AuCl_4^-$ stirred with HSAF without MOPS (◇). Reactions were monitored at 530 nm.

the timescale of minutes. Interestingly, $AuCl_4^-$ reduction was measurably faster in the absence of HSAF, but the absorption signal quickly decreased in this case, indicating the formation and precipitation of insoluble gold colloids. Reduction of $AuCl_4^-$ in the presence of HSAF produced a stable SPR band in aqueous solution, again indicating the stabilizing role of the protein. When stored at 4 °C in buffered solution, Au-HSAF samples remained stable for several months.

It is noteworthy that the formation of gold nanoparticles via the reaction between $AuCl_4^-$ and MOPS in the absence of other stabilizing agents has been recently reported [59,60]. The reduction of Au^{3+} by Good's buffers such as MOPS was shown to occur in 1-electron steps, Au(III) → Au(II) → Au(I) → Au(0), with the buffer serving as a mild reducing agent. Electrochemical experiments identified a single anodic peak for MOPS ~ +800 mV vs. Ag/AgCl electrode. The production of soluble gold nanoparticles in these reports instead of bulk gold relates to differences in their synthetic procedures, including: (i) lower

concentrations of reagents in solution, (ii) lack of stirring, and (iii) lack of concentrated phosphate salt buffer. In the present study, MOPS is expected to reduce Au^{3+} by similar 1-electron transfer steps. However, the bound protein may affect the redox potential of the gold and in some cases block inner-sphere electron transfer from MOPS to the gold ions, thereby slowing gold nanoparticle formation. It is of considerable benefit that HSAF solubilizes the gold particles formed by MOPS over a much wider range of pH than is possible with just buffer in solution [59,60].

Fig. 4a shows the absorption spectra of Au-HSAF samples reduced by $NaBH_4$ or MOPS, which were characterized by the gold SPR band [19,61]. The SPR band of MOPS-reduced Au-HSAF ($\lambda_{max} = 535$ nm) showed a 5-nm red shift compared to $NaBH_4$-reduced Au-HSAF, with absorption centered at 530 nm. The effect of reducing conditions on the SPR maximum may reflect small differences in particle morphology [35,62] and aggregation state [8]. Light scattering was observed for all $NaBH_4$-reduced gold samples, as evidenced by an elevated baseline in the UV–Vis spectra (Fig. 4). To probe the effects of possible aggregation, we centrifuged the MOPS-reduced gold particles more rigorously, at 13,000 rpm for 10 min. Fig. 5a shows the absorption spectra of MOPS-reduced Au-HSAF products centrifuged at 5000 rpm (solid line) and 13,000 rpm (dashed line). A 9-nm blue shift of the SPR maxima from 535 nm to 526 nm was observed when the sample was centrifuged at the higher rate. The blue shift appeared to be caused entirely by a loss of aggregation, not the isolation of smaller gold particles. A representative TEM image and histogram of the particle sizes of MOPS-reduced Au-HSAF centrifuged at 13,000 rpm are shown in Fig. 5b and c, which showed virtually identical particle size distributions for samples centrifuged at 5000 and 13,000 rpm. These data indicated that for these Au-HSAF particles, the positions of the SPR bands were more sensitive to particle aggregation state than size.

To test whether the exterior surface of ferritin was sufficient for forming stable gold particles in solution, $AuCl_4^-$ was reduced with MOPS under the same conditions using HSF instead of HSAF. We hypothesized that the presence of the HSF iron hydroxide mineral core should have little effect on gold nanoparticle formation. Consistent with this hypothesis, an SPR band of Au-HSF centered at 535 nm was recorded for the MOPS-reduced sample, which agreed with Au-HSAF. However, for reasons that are still under

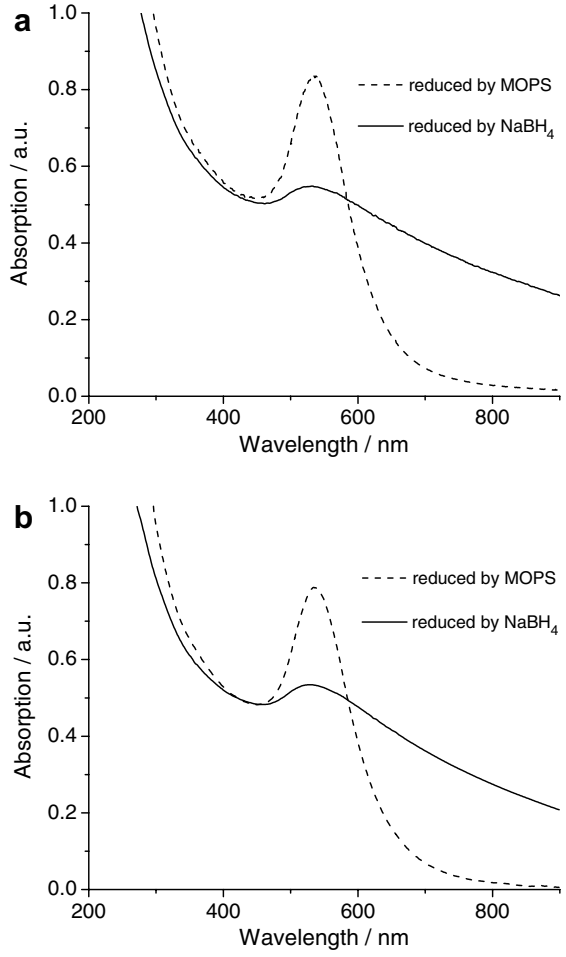

Fig. 4. (a) Absorption spectra of Au-HSAF reduced by $NaBH_4$ (solid line) or MOPS (dashed line) using $AuCl_4^-$ as the gold ion source. (b) Absorption spectra of Au-HSAF reduced by $NaBH_4$ (solid line) or MOPS (dashed line) using $AuCl_3$ as the gold ion source.

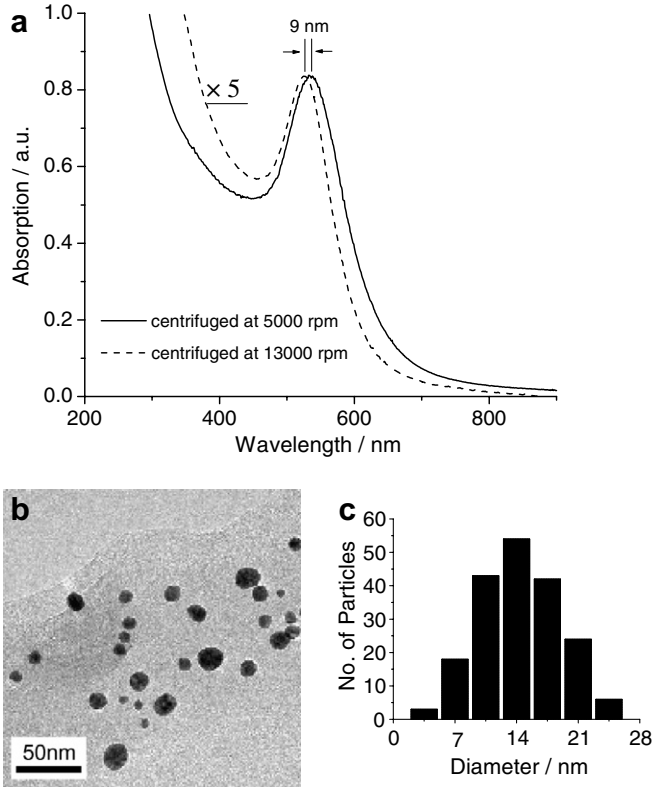

Fig. 5. (a) Absorption spectra of MOPS-reduced Au-HSAF products centrifuged at 5000 rpm (solid line) and 13,000 rpm (dashed line), respectively. (b) TEM image of MOPS-reduced Au-HSAF centrifuged at 13,000 rpm. (c) Histogram of the particle size of the sample in (b) (192 particles analyzed).

investigation, HSF proved to be worse at stabilizing gold nanoparticles in aqueous solution.

Exploring the gold–protein interactions further, we tested whether the negatively charged 3-fold symmetric channels of HSAF were important for gold nanoparticle formation using neutral $AuCl_3$ as the Au^{3+} source. Fig. 4b shows the absorption spectra of Au-HSAF samples reduced by $NaBH_4$ or MOPS, which gave essentially the same results for $AuCl_3$ and $AuCl_4^-$. This indicated that the gold ion source, whether neutral or negatively charged, had little influence on particle formation. These results, together with the TEM data and HSF experiments, supported a model in which gold particles were nucleated on the exterior protein surface.

We also varied gold ion concentrations at three pH values and monitored the intensity of the SPR band, in order to probe a range of conditions for gold nanoparticle formation. At a pH of 6.5, 7.5, and 8.5, we added 1000, 4000, or 7000 eq $AuCl_4^-$ per HSAF and monitored the SPR band upon reduction with either $NaBH_4$ or MOPS. A pH of 7.5 was chosen for subsequent experiments because it represented the most biologically relevant conditions while retaining the ability to synthesize Au^0 nanoparticles in an efficient manner. For both reducing agents, it was found that the SPR intensities were enhanced by increasing from 1000 to 4000 eq $AuCl_4^-$. For 7000 eq $AuCl_4^-$, the SPR intensities decreased in general, more for $NaBH_4$ than when MOPS was the reducing agent. Therefore, 4000 eq $AuCl_4^-$ per HSAF was chosen for synthetic experiments in this paper.

To determine if the gold surface was completely passivated by the protein after reduction, samples of Au-HSAF were prepared with excess gold (10,000 eq) and purified by FPLC. The pure Au-HSAF sample was subsequently incubated with additional HSAF, and the resulting samples were repurified by size-exclusion chromatography. The elution profiles of $NaBH_4$-reduced and MOPS-reduced Au-HSAF samples are shown in Fig. 6. In both cases, FPLC traces monitoring absorbance at 280 nm showed elution peaks at 7.8 mL and 10.6 mL. The solution eluting at 7.8 mL was red but did not precipitate, indicating the presence of gold nanoparticles stabilized by associated HSAF. The peak at 10.6 mL did not show any absorbance at 530 nm and was found by column calibration to correspond to the molecular weight of pure HSAF (~480 kDa) [41]. The majority of the initial $NaBH_4$-reduced Au-HSAF sample precipitated in the column, as evidenced by the small absorption peaks of the eluted material (Fig. 6a), as well as the red residue that remained on the column. However, addition of extra HSAF to these $NaBH_4$-reduced samples greatly increased their stability on the column. The absorption peaks in the case of the MOPS-reduced Au-HSAF were much larger, but were not greatly enhanced by post-reduction addition of HSAF (Fig. 6b). Therefore, we determined that HSAF, with perhaps some contribution from MOPS, was able to passivate the gold surface under slow reduction conditions. Under

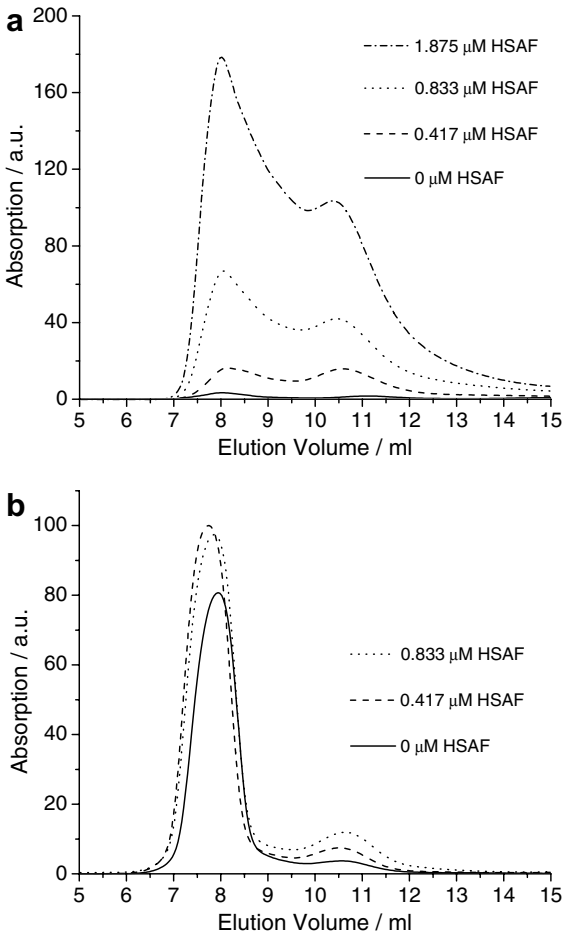

Fig. 6. (a) FPLC elution profiles of $NaBH_4$-reduced Au-HSAF (0.208 μM) with 0 μM HSAF (solid line), 0.417 μM HSAF (dashed line), 0.833 μM HSAF (dotted line) and 1.875 μM HSAF (dashed dotted line). (b) FPLC elution profiles of 0.208 μM MOPS-reduced Au-HSAF with 0 μM HSAF (solid line), 0.417 μM HSAF (dashed line) and 0.833 μM HSAF (dotted line). The traces were scaled such that the area of the gold–protein peak (at 7.8 mL) was proportional to the initial UV–Vis absorbance measurement recorded at 530 nm. FPLC traces were monitored at 280 nm, where both the gold and protein absorb.

conditions of rapid $NaBH_4$ reduction, HSAF capped the gold nanoparticles much less effectively.

The thermal stability of Au-HSAF was investigated by circular dichroism measurements in which the temperature was increased from 4 to 96 °C at a rate of 0.5 °C min^{-1}. Fig. 7 shows the first differential of the ellipticity signal monitoring α-helical content of HSAF at 222 nm. Denaturation or precipitation of the protein at higher temperatures caused a reduction in signal. The melting temperature (T_m) was determined from the midpoint of the melting curve, where the first derivative was the maximum. With melting temperatures of 56 °C ($NaBH_4$-reduced) and 62 °C (MOPS-reduced), Au-HSAF had lower thermal stability than HSAF, $T_m = 71$ °C.

We also examined the stability of Au-HSAF over a wide range of pH values. Fig. 8 shows the pH stability of HSAF and Au-HSAF reduced by $NaBH_4$ or MOPS. Buffered solutions at pH 7.5 were titrated with 1 M HCl and NaOH

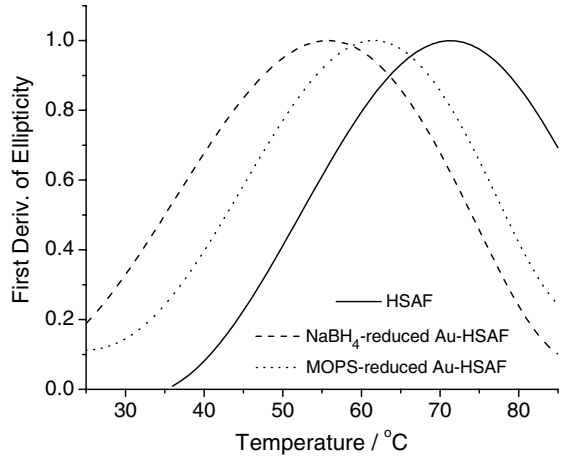

Fig. 7. Thermal stability studies of HSAF (solid line), Au-HSAF reduced by $NaBH_4$ (dashed line) and MOPS (dotted line). The curves were normalized to the same intensity.

to achieve pH 2–12, and centrifuged at 5000 rpm for 10 min to remove any precipitate before spectral characterization. The stability of the Au-HSAF sample as a function of pH was determined by measuring the change of the absorption intensity at 530 nm, while in a control experiment HSAF alone in solution was monitored at 280 nm. The absorbance intensities of all three samples remained generally unchanged at pH values above 7, which indicated comparable stability in alkaline solutions. HSAF effectively stabilized the gold particles in aqueous solution from pH 6 to 12.

When the pH of the solution was gradually lowered from 7 to 2 in increments of 1 pH unit, the absorbance (at 280 nm) decreased for HSAF and even more significantly (at 530 nm) for both Au-HSAF samples. At pH 2, neither Au-HSAF sample showed an SPR band, indicating

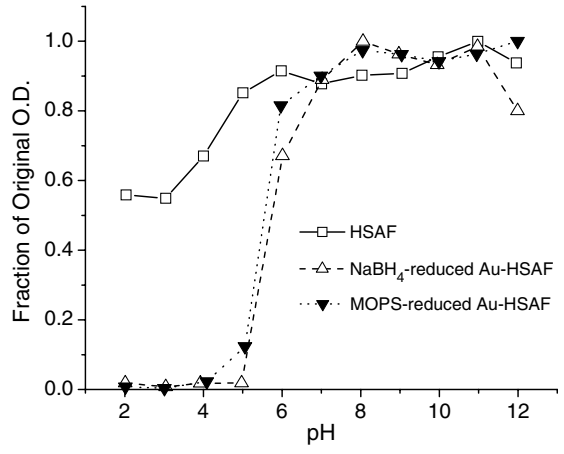

Fig. 8. pH stability of HSAF (□) and Au-HSAF reduced by $NaBH_4$ (△) and MOPS (▼). For HSAF, the normalized absorbance intensities were monitored at 280 nm; for Au-HSAF, the normalized absorbance intensities were monitored at 530 nm. All three curves were normalized to the highest band intensities of each sample to facilitate comparisons of pH stability.

the absence of soluble gold nanoparticles, whereas they both showed protein absorption at 280 nm. Calculations based on the UV–Vis spectra revealed that when lowering the pH from 7 to 2, most of the protein remained in solution for HSAF, $NaBH_4$-reduced Au-HSAF, and MOPS-reduced Au-HSAF samples. Protonation of the exterior protein ligands at low pH should help to dissociate gold from HSAF and yield selective gold precipitation. It is also worth noting that by pH 2, the HSAF 24-mer has dissociated almost completely into its constituent 4-helix bundles [63], which are likely to be less effective at stabilizing gold particles in solution.

As an indirect method for elucidating the protein–metal nanoparticle interactions, we examined the Au-HSAF-catalyzed reduction of 4-nitrophenol by $NaBH_4$. We first tested the catalytic properties of $NaBH_4$-reduced Au-HSAF by adding this sample to an aqueous solution containing 4-nitrophenol and $NaBH_4$. The rapid conversion of the 4-nitrophenol to 4-aminophenol was monitored at 400 nm (Fig. 9a). To exclude the possibility that this reduction might be activated by the protein alone, HSAF was added to 4-nitrophenol and $NaBH_4$ as a control. No change in the phenol absorbance was observed, as shown in Fig. 9b. In the absence of the Au-HSAF catalyst, the absorbance at 400 nm also remained unaltered, indicating that $NaBH_4$ was unable to reduce 4-nitrophenol directly. These results proved that $NaBH_4$-reduced Au-HSAF catalyzed the reduction of 4-nitrophenol by $NaBH_4$. This reaction has been attributed to a gold particle-mediated electron transfer from BH_4^- to 4-nitrophenol [64,65].

Fig. 9b shows the plot of 400-nm absorption versus time for the Au-HSAF-catalyzed reduction of 4-nitrophenol by $NaBH_4$ in the presence of different concentrations of additional HSAF. Because the concentration of $NaBH_4$ added to this system was very high relative to 4-nitrophenol, it was reasonable to assume that the concentration of $NaBH_4$ remained constant during the reaction. Data for $\ln(A_{400})$ were plotted versus time and linear fitting gave a reaction rate constant, $k = 1.66 \times 10^{-2}\,s^{-1}$. With added HSAF (15, 50, and 150 nM), the reaction was slowed ($k = 1.23 \times 10^{-2}$ s^{-1}, 1.04×10^{-2} s^{-1}, and $0.97 \times 10^{-2}\,s^{-1}$), which suggested that the extra protein blocked the access of the substrate to the gold particles, either by increasing the surface coverage or the aggregation state of the particles. This indicated an association process between free HSAF and Au-HSAF in the $NaBH_4$-reduced gold samples, which was consistent with the results of the FPLC study using the same samples.

The catalytic effects of the MOPS-reduced Au-HSAF sample were also examined. Fig. 9b shows a plot of 400-nm absorbance intensity versus time for the Au-HSAF-catalyzed reduction of 4-nitrophenol by $NaBH_4$. In contrast to the previous study, substrate reduction was extremely slow, and adding more HSAF had no noticeable effect on the reaction. The catalyst was presumed to be less accessible to 4-nitrophenol, based on greater coverage of the gold surface with protein, likely in combination with greater

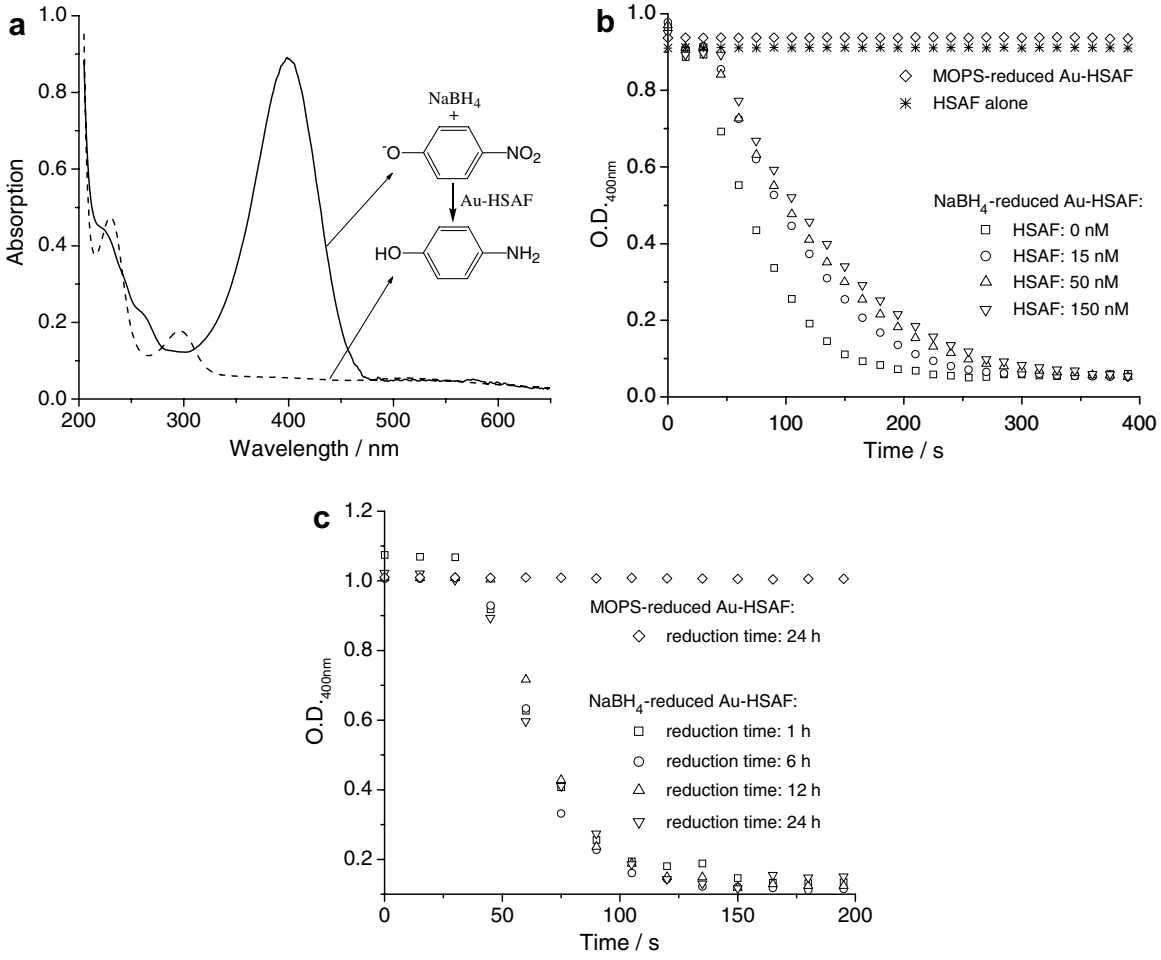

Fig. 9. (a) UV–Vis absorption spectra for the reduction of 4-nitrophenol (50 μM) by $NaBH_4$ (2.5 mM) in the presence of $NaBH_4$-reduced Au-HSAF (5 nM protein) as catalyst. Solid line, initial spectrum; dashed line, final spectrum. (b) Plots of 400-nm absorption versus time for the reduction of 4-nitrophenol (50 μM) by $NaBH_4$ (2.5 mM) using $NaBH_4$-reduced Au-HSAF (5 nM protein) as catalyst in the absence (□) and presence of different concentrations of additional HSAF: 15 nM (○); 50 nM (△); 150 nM (▽); and, using MOPS-reduced Au-HSAF (5 nM protein) as catalyst (◇). Reaction of 4-nitrophenol and $NaBH_4$ in the presence of HSAF alone (5 nM protein, no gold) was included as a control (∗). Values in parentheses represent the final reaction concentrations. (c) Plots of 400-nm absorption versus time for the reduction of 4-nitrophenol (50 μM) by $NaBH_4$ (2.5 mM) using $NaBH_4$-reduced Au-HSAF, which was synthesized with different reduction times: 1 h (□); 6 h (○); 12 h (△); 24 h (▽); and using MOPS-reduced Au-HSAF (◇), which was synthesized with 24-h reduction time.

particle aggregation. Another contributing factor may have been the lower total surface area of the larger MOPS-reduced gold particles, which numbered fewer in solution. The catalysis results corroborated data from UV–Vis spectroscopy, reduction kinetics, FPLC, thermal and pH stability studies, and provided strong evidence for MOPS-reduced Au-HSAF samples being much better passivated at neutral pH than $NaBH_4$-reduced Au-HSAF.

As an indirect measure for whether the Au-HSAF reaction went to completion in the 1-h standard synthetic protocol, the gold-HSAF reaction solution was stirred for between 1 and 24 h after adding either $NaBH_4$ or MOPS. Fig. 9c shows the plots of 400-nm absorption versus time for the reduction of 4-nitrophenol by $NaBH_4$ using $NaBH_4$-reduced Au-HSAF particles that were reacted for 1, 6, 12, or 24 h. Nanoparticles formed in the longer reactions gave virtually identical kinetics for the catalytic reduction of 4-nitrophenol. Au-HSAF prepared by reduction with MOPS for up to 24 h exhibited similarly little catalytic activity (Fig. 9c). This indicated that Au-HSAF particle formation was indeed complete on the 1-h time scale, under both sets of reducing conditions. Data from the previous FPLC experiments showed that for $NaBH_4$-reduced samples, the gold surface remained unpassivated and reactive to additional HSAF. Thus, the catalysis results helped to confirm that the difference in catalytic activity between $NaBH_4$-and MOPS-reduced Au-HSAF was due to intrinsic differences in surface passivation between the two samples, and all of the HSAF in solution was reacted within 1 h during gold reduction and particle formation.

4. Conclusions

In summary, we report a practical method for synthesizing spherical gold nanoparticles using horse spleen apofer-

ritin as the stabilizing agent. Au^{3+} reduction occurred much more rapidly with $NaBH_4$ than MOPS. Gold nanoparticles were shown by TEM to reside on the protein outer surface. A 5-nm red-shifted absorbance of MOPS-reduced gold particles was based mostly on their aggregation in solution; more passivated and less aggregated particles could be obtained through additional centrifugation. Several studies indicated that $NaBH_4$-reduced Au-HSAF was generally less stable than MOPS-reduced samples. This was probably due to rapid reduction by $NaBH_4$, which resulted in fewer stabilizing interactions between the gold and protein. Incomplete gold surface coverage explained why $NaBH_4$-reduced Au-HSAF effectively catalyzed the reduction of 4-nitrophenol by $NaBH_4$. The conjugation of ferritin proteins to metal nanoparticles provides new routes to further particle functionalization and assembly by labeling surface amino acids [66,67]. The techniques employed in this work for studying ferritin–gold nanoparticle assemblies may be readily applied to other protein–metal colloid systems.

Acknowledgements

We thank Doug Yates and Neelima Shah for TEM studies, Feng Gai and Jeffery Saven for access to biophysical instrumentation. This work was supported by a Camille and Henry Dreyfus New Faculty Award and the NSF (CHE 0548188 and DMR-0520020).

References

[1] L.A. Gugliotti, D.L. Feldheim, B.E. Eaton, Science 304 (2004) 850–852.
[2] L.A. Gugliotti, D.L. Feldheim, B.E. Eaton, J. Am. Chem. Soc. 127 (2005) 17814–17818.
[3] D.G. Liu, L.A. Gugliotti, T. Wu, M. Dolska, A.G. Tkachenko, M.K. Shipton, B.E. Eaton, D.L. Feldheim, Langmuir 22 (2006) 5862–5866.
[4] C.F. Monson, A.T. Woolley, Nano Lett. 3 (2003) 359–363.
[5] H.A. Becerril, R.M. Stoltenberg, D.R. Wheeler, R.C. Davis, J.N. Harb, A.T. Woolley, J. Am. Chem. Soc. 127 (2005) 2828–2829.
[6] H.A. Becerril, P. Ludtke, B.M. Willardson, A.T. Woolley, Langmuir 22 (2006) 10140–10144.
[7] J.J. Storhoff, R. Elghanian, C.A. Mirkin, R.L. Letsinger, Langmuir 18 (2002) 6666–6670.
[8] C.A. Mirkin, R.L. Letsinger, R.C. Mucic, J.J. Storhoff, Nature 382 (1996) 607–609.
[9] S.R. Whaley, D.S. English, E.L. Hu, P.F. Barbara, A.M. Belcher, Nature 405 (2000) 665–668.
[10] S.W. Lee, C.B. Mao, C.E. Flynn, A.M. Belcher, Science 296 (2002) 892–895.
[11] M.M. Stevens, N.T. Flynn, C. Wang, D.A. Tirrell, R. Langer, Adv. Mater. 16 (2004) 915–918.
[12] R. Djalali, J. Samson, H. Matsui, J. Am. Chem. Soc. 126 (2004) 7935–7939.
[13] T. Ueno, T. Koshiyama, T. Tsuruga, T. Goto, S. Kanamaru, F. Arisaka, Y. Watanabe, Angew. Chem. Int. Ed. 45 (2006) 4508–4512.
[14] A.S. Blum, C.M. Soto, C.D. Wilson, J.D. Cole, M. Kim, B. Gnade, A. Chatterji, W.F. Ochoa, T.W. Lin, J.E. Johnson, B.R. Ratna, Nano Lett. 4 (2004) 867–870.
[15] T. Takahashi, S. Kuyucak, Biophys. J. 84 (2003) 2256–2263.
[16] S. Srivastava, A. Verma, B.L. Frankamp, V.M. Rotello, Adv. Mater. 17 (2005) 617–621.
[17] J. Yang, M. Mayer, J.K. Kriebel, P. Garstecki, G.M. Whitesides, Angew. Chem. Int. Ed. 43 (2004) 1555–1558.
[18] E. Katz, I. Willner, Angew. Chem. Int. Ed. 43 (2004) 6042–6108.
[19] M.C. Daniel, D. Astruc, Chem. Rev. 104 (2004) 293–346.
[20] Y. Lu, J.W. Liu, Curr. Opin. Biotechnol. 17 (2006) 580–588.
[21] J.W. Liu, Y. Lu, J. Fluoresc. 14 (2004) 343–354.
[22] S.J. Park, T.A. Taton, C.A. Mirkin, Science 295 (2002) 1503–1506.
[23] S.J. Park, A.A. Lazarides, J.J. Storhoff, L. Pesce, C.A. Mirkin, J. Phys. Chem. B 108 (2004) 12375–12380.
[24] A.J. Haes, S.L. Zou, G.C. Schatz, R.P. Van Duyne, J. Phys. Chem. B 108 (2004) 109–116.
[25] E. Hao, G.C. Schatz, J.T. Hupp, J. Fluoresc. 14 (2004) 331–341.
[26] A.J. Haes, C.L. Haynes, A.D. McFarland, G.C. Schatz, R.R. Van Duyne, S.L. Zou, MRS Bull. 30 (2005) 368–375.
[27] C.R. Yonzon, X. Zhang, J. Zhao, R.P. Van Duyne, Spectroscopy 22 (2007) 42–56.
[28] P. Kohli, M. Wirtz, C.R. Martin, Electroanalysis 16 (2004) 9–18.
[29] M. Wirtz, S.F. Yu, C.R. Martin, Analyst 127 (2002) 871–879.
[30] J.W. Liu, Y. Lu, J. Am. Chem. Soc. 125 (2003) 6642–6643.
[31] J.W. Liu, Y. Lu, Anal. Chem. 76 (2004) 1627–1632.
[32] R.A. Reynolds, C.A. Mirkin, R.L. Letsinger, J. Am. Chem. Soc. 122 (2000) 3795–3796.
[33] J. Chen, F. Saeki, B.J. Wiley, H. Cang, M.J. Cobb, Z.Y. Li, L. Au, H. Zhang, M.B. Kimmey, X.D. Li, Y. Xia, Nano Lett. 5 (2005) 473–477.
[34] J.Y. Chen, B. Wiley, Z.Y. Li, D. Campbell, F. Saeki, H. Cang, L. Au, J. Lee, X.D. Li, Y.N. Xia, Adv. Mater. 17 (2005) 2255–2261.
[35] M.M. Alvarez, J.T. Khoury, T.G. Schaaff, M.N. Shafigullin, I. Vezmar, R.L. Whetten, J. Phys. Chem. B 101 (1997) 3706–3712.
[36] A.G. Tkachenko, H. Xie, D. Coleman, W. Glomm, J. Ryan, M.F. Anderson, S. Franzen, D.L. Feldheim, J. Am. Chem. Soc. 125 (2003) 4700–4701.
[37] A.C. Templeton, D.E. Cliffel, R.W. Murray, J. Am. Chem. Soc. 121 (1999) 7081–7089.
[38] S. Aime, L. Frullano, S.G. Crich, Angew. Chem. Int. Ed. 41 (2002) 1017–1019.
[39] J.M. Dominguez-Vera, J. Inorg. Biochem. 98 (2004) 469–472.
[40] E. Simsek, M.A. Kilic, J. Magn. Magn. Mater. 293 (2005) 509–513.
[41] E.C. Theil, Annu. Rev. Biochem. 56 (1987) 289–315.
[42] H. Yoshimura, Colloids Surf. A 282 (2006) 464–470.
[43] A. Treffry, E.R. Bauminger, D. Hechel, N.W. Hodson, I. Nowik, S.J. Yewdall, P.M. Harrison, Biochem. J. 296 (1993) 721–728.
[44] S. Pead, E. Durrant, B. Webb, C. Larsen, D. Heaton, J. Johnson, G.D. Watt, J. Inorg. Biochem. 59 (1995) 15–27.
[45] M. Okuda, K. Iwahori, I. Yamashita, H. Yoshimura, Biotechnol. Bioeng. 84 (2003) 187–194.
[46] K. Yoshizawa, K. Iwahori, K. Sugimoto, I. Yamashita, Chem. Lett. 35 (2006) 1192–1193.
[47] J. Turkevich, P.C. Stevenson, J. Hillier, Discuss. Faraday Soc. 11 (1951) 55–74.
[48] G. Frens, Nature Phys. Sci. 241 (1973) 20–22.
[49] M. Brust, M. Walker, D. Bethell, D.J. Schiffrin, R. Whyman, J. Chem. Soc. Chem. Commun. (1994) 801–802.
[50] A.C. Templeton, S.W. Chen, S.M. Gross, R.W. Murray, Langmuir 15 (1999) 66–76.
[51] J.L. Burt, C. Gutierrez-Wing, M. Miki-Yoshida, M. Jose-Yacaman, Langmuir 20 (2004) 11778–11783.
[52] A.V. Singh, B.M. Bandgar, M. Kasture, B.L.V. Prasad, M. Sastry, J. Mater. Chem. 15 (2005) 5115–5121.
[53] T.C. Chiu, S.H. Chiou, M.M. Hsieh, Y.T. Chen, H.T. Chang, J. Nanosci. Nanotechnol. 5 (2005) 2128–2132.
[54] Y.G. Kim, S.K. Oh, R.M. Crooks, Chem. Mater. 16 (2004) 167–172.
[55] T.G. Schaaff, G. Knight, M.N. Shafigullin, R.F. Borkman, R.L. Whetten, J. Phys. Chem. B 102 (1998) 10643–10646.
[56] J.M. Slocik, M.O. Stone, R.R. Naik, Small 1 (2005) 1048–1052.
[57] D. Ensign, M. Young, T. Douglas, Inorg. Chem. 43 (2004) 3441–3446.
[58] M.M. Bradford, Anal. Biochem. 72 (1976) 248–254.
[59] J. Xie, J.Y. Lee, D.I.C. Wang, Chem. Mater. 19 (2007) 2823–2830.

[60] A. Habib, M. Tabata, Y.G. Wu, Bull. Chem. Soc. Jpn. 78 (2005) 262–269.
[61] S. Link, M.A. El-Sayed, J. Phys. Chem. B 103 (1999) 8410–8426.
[62] S. Mandal, S.K. Arumugam, S.D. Adyanthaya, R. Pasricha, M. Sastry, J. Mater. Chem. 14 (2004) 43–47.
[63] R.R. Crichton, C.F.A. Bryce, Biochem. J. 133 (1973) 289–299.
[64] K. Hayakawa, T. Yoshimura, K. Esumi, Langmuir 19 (2003) 5517–5521.
[65] J.C. Liu, G.W. Qin, P. Raveendran, Y. Kushima, Chem. Eur. J. 12 (2006) 2132–2138.
[66] M. Li, S. Mann, J. Mater. Chem. 14 (2004) 2260–2263.
[67] M.L. Flenniken, D.A. Willits, A.L. Harmsen, L.O. Liepold, A.G. Harmsen, M.J. Young, T. Douglas, Chem. Biol. 13 (2006) 161–170.
[68] T. Ueno, M. Suzuki, T. Goto, T. Matsumoto, K. Nagayama, Y. Watanabe, Angew. Chem. Int. Ed. 43 (2004) 2527–2530.
[69] N. Galvez, P. Sanchez, J.M. Dominguez-Vera, Dalton Trans. (2005) 2492–2494.
[70] N. Galvez, P. Sanchez, J.M. Dominguez-Vera, A. Soriano-Portillo, M. Clemente-Leon, E. Coronado, J. Mater. Chem. 16 (2006) 2757–2761.
[71] T. Douglas, D.P.E. Dickson, S. Betteridge, J. Charnock, C.D. Garner, S. Mann, Science 269 (1995) 54–57.
[72] F.C. Meldrum, B.R. Heywood, S. Mann, Science 257 (1992) 522–523.
[73] F.C. Meldrum, V.J. Wade, D.L. Nimmo, B.R. Heywood, S. Mann, Nature 349 (1991) 684–687.
[74] J.F. Hainfeld, Proc. Natl. Acad. Sci. USA 89 (1992) 11064–11068.
[75] F.C. Meldrum, T. Douglas, S. Levi, P. Arosio, S. Mann, J. Inorg. Biochem. 58 (1995) 59–68.
[76] B. Zhang, J.N. Harb, R.C. Davis, J.W. Kim, S.H. Chu, S. Choi, T. Miller, G.D. Watt, Inorg. Chem. 44 (2005) 3738–3745.
[77] T. Douglas, V.T. Stark, Inorg. Chem. 39 (2000) 1828–1830.
[78] K.K.W. Wong, S. Mann, Adv. Mater. 8 (1996) 928–932.
[79] I. Yamashita, J. Hayashi, M. Hara, Chem. Lett. 33 (2004) 1158–1159.
[80] K. Iwahori, K. Yoshizawa, M. Muraoka, I. Yamashita, Inorg. Chem. 44 (2005) 6393–6400.